epl draft

Single polymer adsorption in shear: flattening versus hydrodynamic lift and surface potential corrugation effects

A. Serr, C. Sendner, F. Müller, T. R. Einert and R. R. Netz

Physics Department, TU Munich - 85748 Garching, Germany

Abstract. - The adsorption of a single polymer to a flat surface in shear is investigated using Brownian hydrodynamics simulations and scaling arguments. Competing effects are disentangled: in the absence of hydrodynamic interactions, shear drag flattens the chain and thus enhances adsorption. Hydrodynamic lift on the other hand gives rise to long-ranged repulsion from the surface which preempts the surface-adsorbed state via a discontinuous desorption transition, in agreement with theoretical arguments. Chain flattening is dominated by hydrodynamic lift, so overall, shear flow weakens the adsorption of flexible polymers. Surface friction due to small-wavelength surface potential corrugations is argued to weaken the surface attraction as well.

The adsorption of polymers on surfaces is at the base of many applications such as surface modification, colloidal stabilization and flocculation. By tailoring adsorption properties, polymer additives can be used as lubricants, adhesives, strength enhancing agents or coagulants. Many experimental and theoretical investigations on the basic research level exist, see [1] for references. The theoretical foundation for polymer adsorption has been laid down by de Gennes [2]. Recent works fine-tuned the microscopic picture and addressed the adsorption of charged or stiff polymers [3,4].

Although it was realized early that non-equilibrium effects are very relevant for polymer adsorption because of the long relaxation times [2], most theoretical and experimental work concentrated on equilibrium aspects [1,5]. However, technological applications involving polymer adsorption are typically far from equilibrium. Along the same lines, many biological mechanisms involve adsorption of macromolecules in shear flow, e.g. the initiation of the coagulation cascade involving the van-Willebrand-factor [6] or the adsorption of E. coli on surfaces [7]. Non-equilibrium aspects of polymer adsorption receive growing attention both from the experimental [8–15] and theoretical point of view [16–22] but are still less well understood than the equilibrium case. In the context of the current theoretical investigation, two opposing effects are relevant: A polymer that is either pulled laterally by a terminally exerted force [25] or subject to shear [15,22] at an adsorbing surface is flattened. In the absence of hydrodynamic interactions, this has been found to *enhance* adsorption in simulations [17,19]. On the other hand, hydrodynamic effects generate a shear-dependent long-ranged lift force that decays quadratically with distance from the surface for dumbbell models [23] as well as for stiff and flexible polymers [24,26] which in simulations has been found to *weaken* polymer adsorption [20]. In the present work we disentangle those opposing aspects and consider flexible polymer at adsorbing surfaces in shear flow using simulations and theory: In the absence of hydrodynamics, we rationalize the shear-induced flattening of the chain and the adsorption enhancement observed in simulations by linear-response theory. As we turn on hydrodynamic interactions in simulations, long-ranged hydrodynamic lift effects dominate over chain flattening effects and lead to chain desorption via a discontinuous transitions, as predicted by scaling arguments. An analysis of a single-particle model based on the Fokker-Planck equation suggests that lateral motion over a surface with an inhomogeneous or corrugated potential weakens the effective attraction, in line with previous simulations [21] Our overall conclusion is that shear flow weakens the adsorption of flexible polymer chains on planar surfaces.

In the simulations, a polymer is composed of N spherical beads with diameter a. Neglecting particle inertia, the time evolution of the position of monomer i obeys the
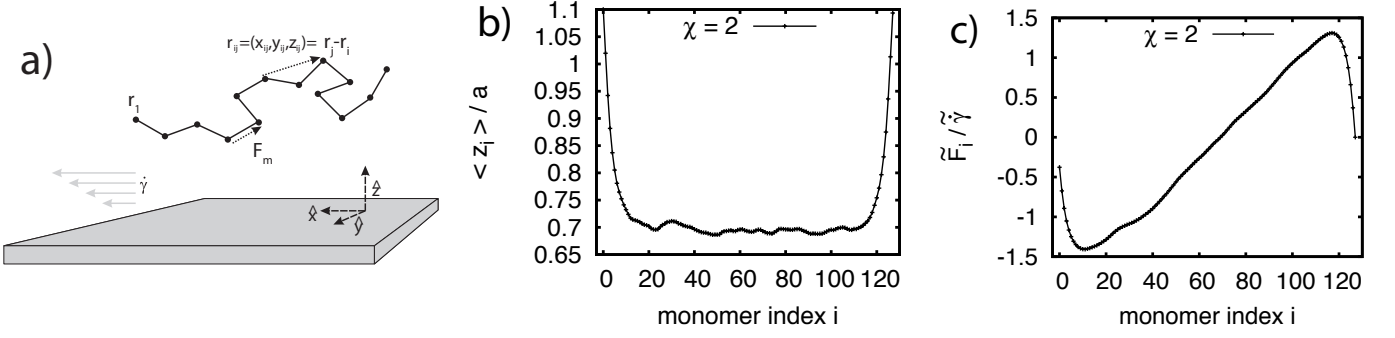
Fig. 1: a) Schematic picture of the polymer model for non-equilibrium adsorption in shear. The $\hat{z}$ axis coincides with the surface normal. The position of monomer i is denoted as $\boldsymbol{r}_i = (x_i, y_i, z_i)$, the distance between two monomers i and j as $\boldsymbol{r}_{ij} = (x_{ij}, y_{ij}, z_{ij}) = \boldsymbol{r}_j - \boldsymbol{r}_i$. The force $\boldsymbol{F}_m$ is the force exerted by monomer $m+1$ on monomer m. A simple shear flow in $\hat{x}$ direction acts with shear rate $\dot{\gamma}$. b) The mean height profile $\{z_i/a\}$, $i = 1\ldots 128$ as a function of the monomer index i for a 128mer obtained from equilibrium BD simulations at the adsorption strength $\chi = 2$ and decay length $\tilde{\kappa}^{-1} = 1/2$. c) The mean rescaled and averaged lateral force $\tilde{F}_i/\dot{\tilde{\gamma}} = \langle F_i^{(x)} \rangle \mu_0/\dot{\gamma} a$ as a function of the bond index i for a 128mer. The profiles are obtained from the height distributions shown in b) via eq. (7).

Langevin equation [27]

$$\dot{\mathbf{r}}_i(t) = -\sum_{j=1}^{N} \boldsymbol{\mu}_{ij} \boldsymbol{\nabla}_{r_j} U(\{\mathbf{r}_N\}) +$$

$$k_B T \sum_j \boldsymbol{\nabla}_{r_j} \boldsymbol{\mu}_{ij} + \dot{\gamma} z_i \hat{\boldsymbol{e}}_x + \boldsymbol{\xi}_i(t), \quad (1)$$

a typical setup of the simulation is shown in fig. 1(a). Hydrodynamic effects are incorporated via the mobility matrix $\boldsymbol{\mu}_{ij}$ which is obtained from the Green's function $\mathbf{G}^W(\mathbf{r}_i, \mathbf{r}_j)$ of the Stokes equation that satisfies the no-slip condition on a planar boundary [26,28]. Performing a multipole expansion to second order in terms of the bead diameter a, which is accurate for bead-bead and bead-surface separations larger than $\approx 2a$, we write [29]

$$\boldsymbol{\mu}_{ij}(\mathbf{r}_i, \mathbf{r}_j) = \left[1 + \frac{a^2}{24} \boldsymbol{\nabla}_{\mathbf{r}_i}^2\right] \left[1 + \frac{a^2}{24} \boldsymbol{\nabla}_{\mathbf{r}_j}^2\right] \mathbf{G}^W(\mathbf{r}_i, \mathbf{r}_j) \quad (2)$$

for $i \neq j$. The self mobility tensor $\boldsymbol{\mu}_{ii}$ is obtained in the limit $\mathbf{r}_i \to \mathbf{r}_j$ and regularized far away from the surface and set equal to the bulk sphere mobility $\mu_0 = 1/(3\pi\eta a)$ [29]. This hydrodynamic treatment is valid in the incompressible low-Reynolds-number limit and assumes instantaneous propagation of hydrodynamic effects, which is accurate for most experimentally relevant situations. Effects due to the discreteness of water molecules are in fact negligible for all but sub-nanometer length scales [30]. In the free-draining simulations, the mobility tensor is set to be diagonal and constant in space,

$$\boldsymbol{\mu}_{ij}(\mathbf{r}_i, \mathbf{r}_j) = \delta_{ij} \mu_0 \mathbf{1} \quad (3)$$

where $\mathbf{1}$ is the diagonal unitary tensor. The externally imposed flow is a linear shear with shear rate $\dot{\gamma}$. For the Brownian dynamics simulations, we use the rescaled, dis-

crete version [31] of eq. (1),

$$\tilde{\mathbf{r}}_i(t + \Delta t) - \tilde{\mathbf{r}}_i(t) = -\sum_{j=1}^{N} \tilde{\boldsymbol{\mu}}_{ij} \boldsymbol{\nabla}_{\tilde{r}_j} u(\{\tilde{\mathbf{r}}_N\})$$

$$+ \sum_j \boldsymbol{\nabla}_{\tilde{r}_j} \tilde{\boldsymbol{\mu}}_{ij} + \tilde{\mu}_0 \dot{\tilde{\gamma}} \tilde{z}_i \hat{\boldsymbol{e}}_x + \tilde{\boldsymbol{\xi}}_i(t). \quad (4)$$

All lengths are scaled by the bead diameter, $\tilde{\mathbf{r}} = \mathbf{r}/a$ and energies by thermal energy, $u(\{\tilde{\mathbf{r}}_N\})k_B T = U(\{\mathbf{r}_N\})$ which leads to rescaled mobilities $\tilde{\boldsymbol{\mu}}_{ij} = \boldsymbol{\mu}_{ij}\Delta t k_B T/a^2$ with timestep Δt and to a rescaled shear rate $\dot{\tilde{\gamma}} = \dot{\gamma} a^2/(k_B T \mu_0)$. The random velocities which couple the system to a heat bath are modeled with Gaussian white noise and fulfill the fluctuation dissipation theorem, $\langle \tilde{\boldsymbol{\xi}}_i(t)\tilde{\boldsymbol{\xi}}_j(t') \rangle = 2\tilde{\boldsymbol{\mu}}_{ij}\delta(t - t')$. The rescaled time step $\tilde{\mu}_0 = \mu_0 \Delta t k_B T/a^2$ must be chosen small enough such that the bead displacement per time step is small compared to the bead radius. The total potential $u = u_{\text{surf}} + u_{\text{poly}}$ consists of bead-bead interactions

$$u_{\text{poly}} = k/2 \sum_i \left(\tilde{r}_{ii+1} - 1\right)^2 + \epsilon \sum_{i<j} \left(\tilde{r}_{ij}^{-12} - 2\tilde{r}_{ij}^{-6}\right), \quad (5)$$

where $\tilde{r}_{ij} = |\tilde{\boldsymbol{r}}_j - \tilde{\boldsymbol{r}}_i|$ is the rescaled monomer distance. The first term ensures the chain connectivity by harmonic bonds around the equilibrium length a with a rescaled spring constant $k = 200$, the second is a truncated Lennard-Jones potential with a rescaled parameter $\epsilon = 2$ which is only used for $\tilde{r}_{ij} < 1$ to avoid overlap of the chain. For the attraction between surface and monomers an exponentially decaying potential is used,

$$u_{\text{surf}} = -\chi \sum_i \exp\left(-\tilde{\kappa}\tilde{z}_i\right), \quad (6)$$

where $\tilde{\kappa}^{-1} = \kappa^{-1}/a$ and χ are the rescaled decay length and the rescaled interaction parameter, respectively. For
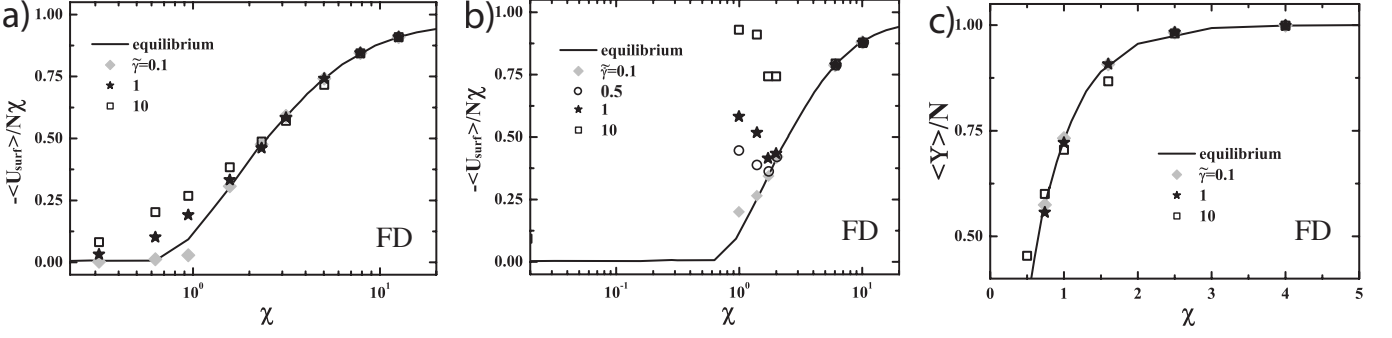
Fig. 2: Free draining (FD) results. a) Simulation results for the mean normalized adsorption potential $-\langle u_{\mathrm{surf}}\rangle/N\chi$ for a 128mer as a function of the surface interaction parameter χ at various shear rates $\dot{\tilde\gamma}$. b) Results from the linear-response theory in which the lateral stretching force distribution due to shear is calculated from the equilibrium monomer height distribution via eq. (7) and used to derive the effective adsorption strength via eq. (10), see text for details. The linear response theory captures the shear-induced adsorption enhancement only qualitatively. c) Fraction of adsorbed monomers $\langle\Upsilon\rangle/N$ from simulations. A monomer i is defined adsorbed if $\tilde{z}_i < \tilde\kappa^{-1}$.

electrostatically driven adsorption, the interaction parameter χ can be interpreted as the product of surface and polymer charge density and the decay length κ^{-1} as the screening length. We use the exponential potential as a generic form to study short-ranged surface attraction and have in mind also hydrophobic or van-der-Waals interactions. To make it very short-ranged, we use $\tilde\kappa^{-1} = 1/2$. We also include a hard wall interaction of the monomers at the wall-liquid boundary, i.e. $u_{\mathrm{surf}}(\tilde{z}_i < 0) = \infty$.

We use a rescaled time step of $\tilde\mu_0 = 10^{-4}$ and simulate for at least 10^8 simulation steps. The first 20 % of these steps are disregarded for equilibration. Every 10^3 steps the configuration is recorded. Data are obtained by block-averaging, statistical errors are obtained from the standard deviation of blocks and only shown when larger than the symbol size. Simulations are performed for polymers of typical length $N = 64$ or 128 and for different values of the adsorption strength ($\chi = 10^{-4}\ldots 10^2$).

We first briefly review the adsorption of a single polymer in equilibrium. In thermodynamic equilibrium, *any* polymer of *finite* length will desorb from an adsorbing surface into the semi-infinite half-space, no matter how strong the adsorption potential is. However, by carefully choosing polymer length and simulation duration, information about polymer adsorption in the asymptotic limit of an infinitely long polymer can be obtained. This is so because a finite-time window exists within which an adsorbed polymer of finite length has enough time to equilibrate its conformation but at the same time stays trapped in the surface adsorption potential. In fact, this time window widens with increasing monomer number N, or, conversely, shrinks for too short polymers.

The transition between the adsorbed and desorbed state can be quantified with different observables, e.g. the adsorption potential energy [5], the polymer mean height [4] or the number of adsorbed monomers [16]. In fig. 2(a) we plot the mean adsorption potential per monomer, $-\langle u_{\mathrm{surf}}/\chi N\rangle$, calculated from eq. (6), for a 128mer as a

function of χ. In the thermodynamic limit $N \to \infty$ this observables is expected to go to zero in a continuous fashion at the adsorption transition.

Next we establish a simple linear response theory for the flattening of a chain in shear flow. For simplicity, we consider a freely jointed chain (FJC) and neglect hydrodynamic interactions and excluded-volume interaction between beads. We assume the chain to take some average separation from the surface. From eq. (1) the x-component of the velocity of bead i reads $\dot{x}_i = \dot{\gamma}z_i + \mu_0 F_i^{(x)} - \mu_0 F_{i-1}^{(x)} + \xi_i^{(x)}$ where $F_i^{(x)}$ denotes the force that bead $i+1$ exerts on bead i via the bonding potential. By reciprocity, $-F_{i-1}^{(x)}$ is the force that bead $i-1$ exerts on bead i and the boundary condition reads as $F_N^{(x)} = F_0^{(x)} = 0$. By averaging this equation, the random force disappears and we obtain $\langle\dot{x}_i\rangle = \dot{\gamma}\langle z_i\rangle + \mu_0\langle F_i^{(x)}\rangle - \mu_0\langle F_{i-1}^{(x)}\rangle$. In the stationary state, all monomers have the same average velocity equal to the mean chain velocity, $\langle\dot{x}_1\rangle = \langle\dot{x}_2\rangle = \cdots$, which furnishes $N - 1$ equations. Solving for the forces, we obtain

$$\langle F_i^{(x)}\rangle = -\frac{\dot{\gamma}}{\mu_0}\sum_{j=1}^{i}\langle z_j - \sum_{k=1}^{N} z_k/N\rangle \qquad (7)$$

which constitutes an exact relation between the average chain height profile and the mean forces acting on the polymer bonds.

According to standard polymer statistical mechanics, the mean extension of a FJC bond along the pulling direction is $\langle\tilde{x}_{ii+1}\rangle \equiv \langle\tilde{x}_{i+1}-\tilde{x}_i\rangle = \mathcal{L}(\tilde{F}_i)$ where $\mathcal{L}(x) = \coth x - x^{-1}$ is the Langevin function and $\tilde{F}_i = a\langle F_i^{(x)}\rangle/k_B T$ is a short-hand notation for the rescaled average x-component of the bond force. Likewise, the second moment is given by $\langle\tilde{x}_i^2\rangle = 1 - 2\mathcal{L}(\tilde{F}_i)/\tilde{F}_i$ [25]. If we neglect effects of the surface, the two perpendicular directions, $\hat{y}$ and $\hat{z}$, are equivalent and the mean squared extension perpendicular to the pulling direction is

$$\langle\tilde{z}_i^2\rangle = \left(1 - \langle\tilde{x}_i^2\rangle\right)/2 = \mathcal{L}(\tilde{F}_i)/\tilde{F}_i \qquad (8)$$
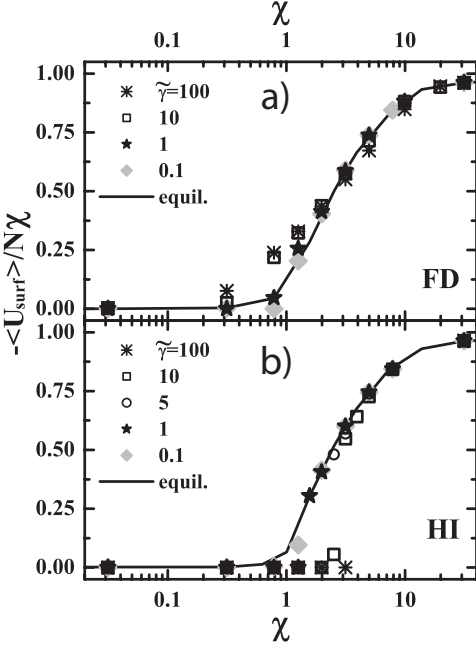
Fig. 3: Mean normalized adsorption potential $-\langle u_{\mathrm{surf}}\rangle/N\chi$ for a 64mer as a function of the surface interaction parameter χ in equilibrium (solid lines) and for various shear rates $\dot{\tilde{\gamma}} = \dot{\gamma}a^2/\mu_0 k_{\mathrm{B}}T$. a) Results from free-draining (FD) BD simulations and b) from hydrodynamic (HI) simulations. In contrast to the FD the HI simulations show weaker adsorption and a discontinuous desorption transition.

with the asymptotic limits $\langle \tilde{z}_i^2 \rangle \overset{\tilde{F}_i \ll 1}{\longrightarrow} 1/3$ for weak force and $\langle \tilde{z}_i^2 \rangle \overset{\tilde{F}_i \gg 1}{\longrightarrow} 1/|\tilde{F}_i|$ for strong force. Since the root mean squared bond radius defines the Kuhn length, we can in the presence of the lateral pulling force define an effective Kuhn length in $\hat{z}$ direction by $a_{\mathrm{eff},i}^2 = 3a^2\mathcal{L}(\tilde{F}_i)/\tilde{F}_i$. In fact, since the force varies along the chain contour, it is useful to define the renormalized Kuhn length as an average over all bonds,

$$\bar{a}_{\mathrm{eff}}^2 = \frac{3a^2}{N-1}\sum_{i=1}^{N-1}\frac{\mathcal{L}(\tilde{F}_i)}{\tilde{F}_i}. \qquad (9)$$

For illustration we show in fig. 1(b-c) the height profile and the force profile at $\chi = 2$. Due to the symmetry of the mean height profile $\langle z_i \rangle$ of the chain and since the chain ends have a larger separation from the surface than the chain middle, according to eq. (7), the force vanishes on the middle and terminal bonds and its magnitude is maximal in between. Note that a non-zero bond force profile would even arise for e.g. polymer loops where by symmetry the mean height profile is flat, caused by chain fluctuation around the mean (a mechanism not pursued further in this paper). Based on the mapping of the problem of a single polymer at an adsorbing surface onto the equivalent problem of a quantum particle at an adsorbing wall [32], the only remaining scaling variable in the problem turns

out to be the effective adsorption strength

$$\chi_{\mathrm{eff}} = \chi a^2/\bar{a}_{\mathrm{eff}}^2. \qquad (10)$$

This gives a direct clue as to how the chain flattening enhances chain adsorption.

As exemplary case we show in fig. 2(a) the mean normalized adsorption potential $-\langle u_{\mathrm{surf}}\rangle/(N\chi)$ for a 128mer from free-draining simulations as a function of the adsorption strength χ for the equilibrium case (solid line) and for different shear rates $\dot{\tilde{\gamma}}$ (symbols). For low values of the adsorption strength χ we note shear-enhanced adsorption in agreement with previous free-draining simulations [17,19]. At large values of χ the adsorption behaviour is not modified. Intuitively, one might expect peeling and tumbling effects to reduce adsorption at strong shearing, but nothing of this sort is seen. In fig. 2c we show the fraction of adsorbed monomers or trains, $\langle \Upsilon \rangle/N$, where a monomer counts as adsorbed when its height is less than the adsorption screening length, $\tilde{z}_i < \tilde{\kappa}^{-1}$ in the strong adsorption regime. Almost no influence of shear is seen. This is easily understood when taking the effects of chain flattening into account. For high adsorption strengths, the polymer adopts a flat configuration with long trains and only few, small loops. The stretching forces acting on the polymer bonds are low and chain flattening is negligible and thus the enhanced adsorption mechanism discussed previously does not come into play. On the other hand, close to the desorption transition loops proliferate and experience stronger shear forces, which leads to chain flattening and thus enhanced polymer adsorption. On the linear-response level, the configuration and adsorption energy of a chain in shear can be approximated by the equilibrium configuration of a chain (i.e. without shear) with the adsorption strength χ replaced by χ_{eff} given by eq. (10). The result of this procedure is shown in fig 2(b). The linear prediction qualitatively captures the shear-induced adsorption enhancement but grossly overestimates the effect. In fact, linear response breaks down at strong shear flows since the resulting chain flattening of the chain very efficiently decreases the shear effects, this is even more enhanced by the stronger adsorption of the flattened chain. The linear theory can in principle be self-consistently improved, which we do not pursue since in the following we show that hydrodynamic lift effects dominate chain flattening.

In fig. 3 we plot the rescaled adsorption potential $-\langle u_{\mathrm{surf}}\rangle/N\chi$ as a function of the adsorption strength χ for the equilibrium case and various shear rates for chains of length $N = 64$. In a) we show the results from free-draining (FD) simulations, in b) we show data for the exact same parameters using full hydrodynamic interactions (HI). As expected, the equilibrium results (solid lines) from both methods coincide within the precision of the simulations. For moderate shear rates the HI simulations quantitatively confirm the results obtained in the FD case. For elevated shear rates, however, the transition into the
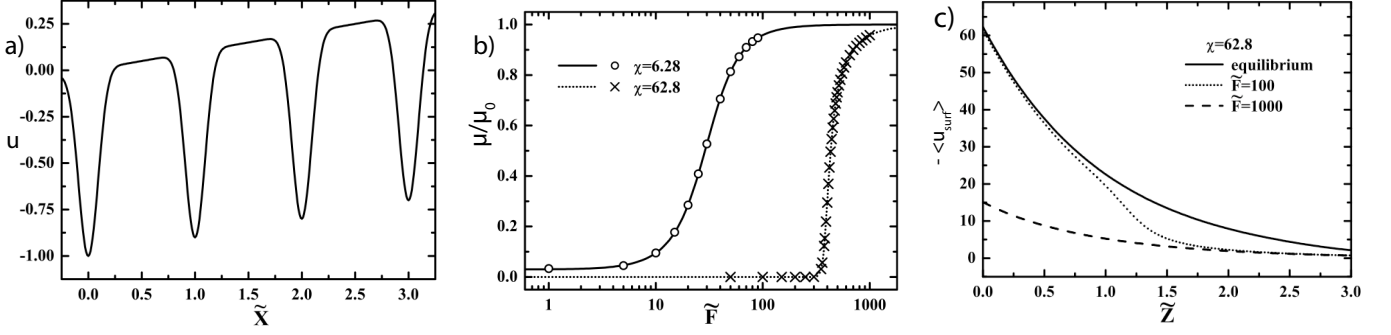
Fig. 4: (a) Potential energy u of a single particle at fixed height $\tilde{z} = 0$ in a surface potential eq. (11) and pulled with a rescaled force of $\tilde{F} = -0.1$. The surface interaction strength is chosen as $\chi = 1$, corrugation power is $\beta = 6$. (b) Average mobilities μ/μ_0 for a single particle pulled through a corrugated potential eq. (11) as a function of the rescaled pulling force $\tilde{F} = Fa/k_BT$ for fixed particle height $\tilde{z} = 0$, $\beta = 6$, $\tilde{\kappa} = 1$, $\chi = 6.28$ and $\chi = 62.8$. Data points are taken from simulations, the lines from Fokker-Planck theory eq. (12). (c) Average surface potential $-\langle u_{\text{surf}} \rangle$ for a single particle as a function of its surface separation $\tilde{z}$ from stationary solutions of the Fokker-Planck eq. (12) with surface potential parameters $\tilde{\kappa} = 1$, $\beta = 6$, and $\chi = 62.8$. For intermediate force $\tilde{F} = 100$ the average potential crosses over from the equilibrium limit ($\tilde{F} = 0$, solid line) to the high-force limit ($\tilde{F} = 1000$, dashed line) at intermediate separation.

desorbed state changes from continuous (FD) to discontinuous (HI) and the magnitude of the adsorption energy is smaller compared to the equilibrium case. We conclude that hydrodynamic effects weaken adsorption in shear and totally dominate the chain flattening effects seen in the absence of correct hydrodynamic effects.

What is the cause for this drastic hydrodynamic repulsion? It is known that dumbbells [23] as well as stiff rods and flexible polymers [24, 26] close to a flat, non-adsorbing surface in shear experience a repulsive lift force away from the surface. This lift force can be rationalzed by the anisotropy of the hydrodynamic mobility parallel and normal to an elongated object [27] in conjunction with the anisotropically distributed orientation of the object in shear [26]. The resulting potential is long-ranged and decays as $\propto 1/z$ for rods as well as flexible polymers at elevated shear rates [26]. The combination of such a long-ranged repulsive potential with a short-ranged attractive surface adsorption potential is known to turn the adsorption transition of a polymer discontinuous [33]. Our simulations confirm the predicted change in the nature of the transition. In summary, due to the relative weak enhancement of adsorption due to chain flattening observed in free-draining simulations, the hydrodynamic lift repulsion dominates and weakens the adsorption and actually turns the transition discontinuous.

Up to now the adsorbing wall was assumed flat and homogeneous. This is a good approximation for atomically flat surfaces or adsorption driven by hydrophobic interactions since here the surface friction effects are small [34, 35]. Also for charged substrates the assumption of a laterally homogeneous potential is accurate if the screening length is larger than the monomer bond length and the separation between charged sites on the substrate. In all other cases, and in specific for adsorption driven by hydrogen-bonds [35], adsorbing polymers do experience

corrugated potentials the non-equilbrium effects of which will be briefly discussed now. Since the equilibration of a polymer in a corrugated potential landscape including hydrodynamic interactions is by far too demanding from the computer time aspect, we consider the simplistic case of a single monomer dragged by an external force in a one-dimensional corrugated potential. As a straightforward extension of the potential eq. (6) used in the simulations, we consider the total potential $u(\tilde{x}, \tilde{z}) = u_{\text{surf}}(\tilde{x}, \tilde{z}) - \tilde{F}\tilde{x}$ including the corrugated surface potential

$$u_{\text{surf}}(\tilde{x}, \tilde{z}) = -\chi \exp\left(-\tilde{\kappa}\tilde{z}\right) \left[\frac{\cos\left(2\pi\tilde{x}\right) + 1}{2} \right]^{\beta} \quad (11)$$

where the exponent β controls the corrugation steepness, the corrugation wavelength is for simplicity set equal to the monomer diameter a, and the force $\tilde{F}$ leads to particle motion. Here we concentrate on the highly corrugated case $\beta = 6$ shown in fig. 4(a) for $\tilde{z} = 0$, $\tilde{F} = -0.1$ and $\chi = 1$. We consider numerical solutions of the stationary Fokker-Planck (FP) equation [36] $0 = \dot{P}(\tilde{x}, \tilde{t}) = u'(\tilde{x})P'(\tilde{x}, \tilde{t}) + u''(\tilde{x})P(\tilde{x}, \tilde{t}) + P''(\tilde{x}, \tilde{t})$, where $P(\tilde{x}, \tilde{t})$ is the normalized distribution function, the rescaled time is $\tilde{t} = t\mu_0 k_BT/a^2$ and $u'(\tilde{x}) = \partial u(\tilde{x})/\partial \tilde{x}$ denotes a partial derivative w.r.t. $\tilde{x}$ (and similarly for P). Note that $\tilde{z}$ only enters parametrically into the FP equation, i.e., the particle is for illustrative purposes constrained to fixed height $\tilde{z}$ and we therefore dropped the $\tilde{z}$-dependence of the potential. For time-independent potentials consisting of a linear and a part periodic over the interval from $\tilde{x} = 0$ to $\tilde{x} = 1$, the stationary solution is given by [36]

$$P(\tilde{x}) = \frac{e^{-u(\tilde{x})}}{Q} \left[\frac{\int_0^1 d\tilde{x}' e^{u(\tilde{x}')}}{1 - e^{u(1)-u(0)}} - \int_0^{\tilde{x}} d\tilde{x}' e^{u(\tilde{x}')} \right] \quad (12)$$

where Q is the normalization constant. The rescaled mobility follows as $\mu/\mu_0 = \langle \dot{\tilde{x}} \rangle/(\tilde{F}\tilde{\mu}_0) =$

$-\int_0^1 d\tilde{x} u'(\tilde{x}) P(\tilde{x})/(\tilde{F}Q)$ and the average potential energy follows as $\langle u_{\text{surf}} \rangle = \int_0^1 d\tilde{x} u_{\text{surf}}(\tilde{x}) P(\tilde{x})/Q$. In fig. 4(b) the normalized particle mobility μ/μ_0 from the FP solution (shown as lines) compares not surprisingly favorably with the Brownian dynamics simulation results (data points) according to eqs. (3) and (4) at fixed particle height $\tilde{z} = 0$. Data is presented for $\chi = 6.28$ (circles) and $\chi = 62.8$ (crosses). For low external force, the particle mostly sticks to the attractive surface sites and the average mobility is very small. At large forces the average mobility approaches its bulk value and the motion is uniform regardless of the potential corrugation. In fig. 4(c) we show the average potential energy $-\langle u_{\text{surf}} \rangle$ as a function of the vertical height $\tilde{z}$ for fixed surface interaction parameter $\chi = 62.8$ and for different driving forces. For comparison, the equilibrium case (i.e. for vanishing force) is shown as a solid line. For the larger force $\tilde{F} = 1000$ the mobility is not modified (as seen from fig. 4(b) for $\tilde{z} = 0$) by the potential and the particle moves uniformly over the surface, the average potential is therefore a uniform average over the corrugation. In contrast, in equilibrium, the particle mostly samples the potential minima and the magnitude of the mean potential is much larger. For intermediate force $\tilde{F} = 100$ an interesting phenomenon appears: For small values of $\tilde{z}$ the particle sticks to the potential minima and the average potential is close to the equilibrium case. With increasing height $\tilde{z}$ the lateral confinement due to the potential is weakened, the mobility increases, and the average potential crosses over to the high-force limit. This means that the effective potential in the presence of a lateral driving force becomes more short-ranged, under the influence of shear where the driving force increases with distance from the surface this effects will be even more pronounced.

For polymer adsorption in shear this means that potential corrugations will in the presence of lateral force or shear tend to weaken the attraction when compared to the equilibrium case. Neglecting the enhanced friction close to the surface, which could lead to chain flattening effects, our tentative conclusion is that potential corrugation will act similarly as hydrodynamic lift effects and favor polymer desorption, in line with simulation results for charged polymers [21]. Furthermore, since the effective corrugated surface potential becomes more short-ranged compared to the equilibrium case, the desorption transition should be even more discontinuous compared to a homogeneous surface potential.

Interesting effects left out in the present study include multi-chain effects, chain stiffness effects and structural effects that go beyond modelling chain monomers as a homogenous spheres.

$$* * *$$

REFERENCES

[1] Netz R. R. and Andelman D., *Phys. Rep.*, **380** (2003) 1.
[2] de Gennes P.-G., *Macromolecules*, **14** (1981) 1637.
[3] Fleer G. J. *et al.*, *Polymers at Interfaces* (Chapman & Hall, London) 1998.
[4] Yamakov V. *et al.*, *J. Phys.: Condens. Matter*, **11** (1999) 9907.
[5] Eisenriegler E. *et al.*, *J. Chem. Phys.*, **77** (1982) 6296.
[6] Schneider S.W. *et al.*, *Proc. Nat. Acad. Sci.* , **104** (2007) 7899.
[7] Thomas W.E, Vogel V. and Sokurenko E., *Annu. Rev. Biophys.*, **37** (2008) 399.
[8] Lee J.-J. and Fuller G. G., *J. Coll. Interf. Sci.*, **103** (1985) 569.
[9] McGlinn T. C. *et al.*, *Phys. Rev. Lett.*, **60** (1988) 805.
[10] Besio G. J. *et al.*, *Macromolecules*, **21** (1988) 1070.
[11] Chin S. and Hoagland D. A., *Macromolecules*, **24** (1991) 1876.
[12] Chang S. H. and Chung I. J., *Macromolecules*, **24** (1991) 567.
[13] Nguyen D. *et al.*, *J. Appl. Cryst.*, **30** (1997) 680.
[14] Kim J. H. *et al.*, *Langmuir*, **23** (2007) 755.
[15] He G.-L. *et al.*, *Soft Matter*, **5** (2009) 3014.
[16] Milchev A. and Binder K., *Macromolecules*, **29** (1996) 343.
[17] Manias E. *et al.*, *Mol. Phys.*, **85** (1995) 1017.
[18] Chopra M. and Larson R.G., *J. Rheol.*, **46** (2002) 831.
[19] Panwar A. S. and Kumar S., *J. Chem. Phys.*, **122** (2005) 154902.
[20] Hoda N. and Kumar S., *J. Chem. Phys.*, **127** (2007) 234902.
[21] Hoda N. and Kumar S., *J. Chem. Phys.*, **128** (2008) 164907.
[22] He G.-L., Messina R. and Löwen H., *J. Chem. Phys.*, **132** (2010) 124903.
[23] Ma H. and Graham D., *Phys. Fluids*, **17** (2005) 083103
[24] Usta O.B. *et al.*, *Phys. Rev. Lett.* , **98** (2007) 098301
[25] Serr A. and Netz R.R., *Europhys. Lett.* , **78** (2008) 68006
[26] Sendner C. and Netz R.R., *Europhys. Lett.* , **81** (2008) 54006
[27] Doi M. and Edwards S. F., *The theory of polymer dynamics* (Oxford University Press, New York) 1986.
[28] Blake J. R., *Proc. Camb. Phil. Soc.* , **70** (1971) 303.
[29] Kim Y. W. and Netz R. R., *J. Chem. Phys.* , **124** (2006) 114709.
[30] Sendner C. *et al.*, *Langmuir* , **25** (2009) 10768
[31] Ermak D. L. and McCammon J. A., *J. Chem. Phys.* , **69** (1978) 1352.
[32] Wiegel F. W., *Introduction to Path-Integral Methods in Physics and Polymer Science* (World Scientific, Singapore) 1986.
[33] Lipowsky, R. R. and Nieuwenhuizen T. M., *J. Phys. A* , **21** (1988) L89.
[34] Kühner F. *et al.*, *Langmuir*, **22** (2006) 11180.
[35] Serr A., Horinek D. and Netz R. R., *J. Am. Chem. Soc.*, **130** (2008) 12408.
[36] Risken H., *The Fokker-Planck Equation, Methods of Solution and Applications* (Springer, New York, Berlin, Heidelberg) 1989.